Modulation of the Solution-Cathode Glow-Discharge and Solution-Anode Glow Discharge using a Rotating Magnetic Field

Nicholas Hazel[1], Jaime Orejas Ibanez[2], and Steven Ray[1]*

[1]Department of Chemistry, State University of New York at Buffalo, Buffalo, NY USA 14226

[2]Grupo de Espectroscopía Láseres y Plasmas (GELP), Department of Physics, University of Oviedo, C/ Gonzalo Gutiérrez Quirós s/n, Mieres, Spain 33600

*Author to whom correspondence should be addressed.

Journal of Applied Physics

Abstract

The effects of an external magnetic field on the solution-cathode glow-discharge (SCGD) and solution-anode glow-discharge (SAGD) are investigated. The SCGD is atmospheric-pressure glow discharge sustained between a metal pin and a liquid cathode electrode in the ambient atmosphere, and it is often used for trace elemental analysis by atomic emission spectroscopy. Here, the SCGD is modified to allow an external permanent magnetic field to be applied, either in a static orientation or as a rotating field, as a means of stabilizing the SCGD plasma and modulating atomic emission from the discharge. The effect of the external magnetic field on the physical structure, electrical characteristics, and spectroscopic response of the SCGD and SAGD are investigated. A rotating external magnetic field was found to change both SAGD and SCGD structure and spatial emission pattern. Analytical figures of merit are examined, and a lock in amplifier is used to discriminate analytical atomic emission from background emission, improving limits of detection.

Introduction

The solution-cathode glow-discharge (SCGD) is a liquid-based atmospheric-pressure glow discharge plasma designed primarily for use in atomic emission spectroscopy[1]. The structure of the SCGD shares much in common with other liquid-electrode plasma discharges[2-4]. A high voltage is applied between a pin-type metal electrode and a sample solution, which is introduced as a flowing stream exiting a quartz capillary. The glow discharge formed directly upon the solution surface removes material from the condensed phase liquid and excites the constituent elements to emission, permitting quantitative analysis by atomic emission spectrometry. Several reports have demonstrated that the SCGD is capable of limits of detection for many elements in the range from 0.01-1 ng/mL, which are competitive with those reported for other, more conventional analytical methods such as the inductively coupled plasma-optical emission spectroscopy (ICP-OES)[3]. However, the SCGD holds significant advantages over conventional approaches like ICP-OES in that it uses no supporting gas (e.g. Ar), uses low-power DC potentials (<100W), and produces a relatively simple emission spectra with relatively few background species [3, 5-8]. Recent reports have also demonstrated that the SCGD architecture can be used with reversed polarity (i.e. solution as the anode), forming a solution-anode glow discharge (SAGD) which has been shown to provide lower atomic emission limits of detection for several elements [9] [10]. While the SCGD has been primarily used for atomic spectroscopy, it has also been used for hydride generation[11], nanoparticle synthesis[12], as a detector in ion chromatography [13], for nanoparticle[14] and complex slurry analysis[15], and as an ionization source for molecular mass spectrometry[16].

Like other liquid-plasma discharges, the interface between the SCGD plasma and the condensed-phase liquid is the critical aspect of its efficacy, but is poorly understood. Vibrational and rotational gas temperature measurements have revealed a steep temperature gradient at the plasma/liquid interface (3000K/mm)[17-19]. Measurements of the potential drop across the cathode dark space have estimated a significant electric field exists in the same region of the discharge (>10^6V/m) [1, 20]. Several researchers have hypothesized that the large electric field at the liquid surface leads to formation of liquid jets (i.e. a Taylor cone), which removes sample from the condensed phase into the plasma. Indeed, recent results utilizing low-angle laser scattering to probe the solution-plasma interface have revealed the presence of jets emitting from the liquid[1, 2, 22-24]. The SCGD plasma shares structural similarity with other atmospheric pressure glow discharges in the formation of anode and cathode spot patterns and filamentation[1, 2, 23, 25, 26]. Schwartz and coworkers reported that when the SCGD is imaged on a rapid timescale (100nsec), it is found to be composed of 10-20 individual filaments in contact with the liquid surface[1]. Co-localization of atomic emission from the points where the filaments interact with the liquid suggests that they are critical in the operation of the SCGD[1]. Understanding and controlling these aspects of the SCGD is an important aspect of optimizing this emission source for atomic spectrometry.

Ongoing research seeks to develop the liquid plasma as an analytical system in a way that optimizes quantitative measurement by atomic emission spectroscopy[27]. The most significant difference between the SCGD and other liquid-plasma geometries is this use of a quartz capillary in order to confine the plasma to a restricted cathode area (e.g. 1mm^2)[5, 28]. The restricted cathodic area allows samples to be introduced in an isolated flowing stream, increases power density, and has led to improved limits of detection over prior designs [21]. Similarly, a variety

of plasma powering strategies have also been investigated, including alternating current[29] and high voltage pulses[30], as well novel measurement strategies such as the use of interference filters[31], and spatially-resolved emission measurements[32]. In each instance, such developments are intended to accentuate the capabilities of this simple atomic emission source.

Recently, Zhou and coworkers examined the effect of a static magnetic field on the SCGD and reported a 2-3 times enhancement of emission signal from Cd, Cu, Pb, and Zn solutions [33]. The increase in sensitivity improved the limits of detection of these elements without significant modification to the discharge architecture. External magnetic fields are widely used to modulate plasma characteristics, either by controlling the plasma structure, fundamental characteristics, or for spectroscopic purposes. For example, DC plasma arcs used in emission spectroscopy are often placed within a rotating magnetic field in order to stabilize the discharge structure, greatly improving emission measurement precision[34], and increasing spectral line intensity [35]. Magnetic manipulation of reduced pressure glow discharges was first reported in 1901, and analytical glow discharges have been modified with magnetic fields in order to improve analytical characteristics[36-38] [39], [40, 41]. The Lorentz force (F_L) perturbs charged species in motion, with the electrons being affected to a greater extent than ions due to their lower mass[42]. Under typical conditions in a glow discharge, electrons move towards the anode with a drift velocity (v) that reflects the influence of the local electric field force vector (F_E). Application of the magnetic field imposes an additional Lorentz force as a cross product (F_L=ev X B) where e is the elementary charge, v the drift velocity, and B the magnetic field strength. The vector sum of both force components ($F_E + F_L$) creates a curved path for charged particles according to the right-hand rule. In plasma systems, the mechanism of ambipolar diffusion produces effective drift velocities that are less than free the electron, but greater than an ion. The potential for beneficial effects to the

SCGD in modifying structure, fundamental characteristics, and improving atomic spectroscopy performance by increased emission yield, stabilization of the SCGD plasma, or modification of the rate of material removed from the condensed phase sample is clear.

In this preliminary work we examine the effect of a rotating magnetic field on the SCGD plasma for the first time, and evaluate the utility of the approach for atomic emission spectroscopy. Here, the magnetic field was sustained using a permanent rare-earth magnet in static orientation, or rotated at a set rate (Figure 1). The effects of the Lorentz force on the plasma are examined using optical imaging, electrical characterization, high-speed videography, and spectroscopic analysis. The efficacy of the approach in controlling the chaotic environment around the plasma-liquid interface in the SCGD is evaluated. The results are appraised for potential benefit in atomic emission spectroscopy as a means of modulation to discern atomic emission signal from background emission from the plasma continuum or from specific background interferents.

Experimental

A representation of the SCGD experimental setup is shown in Figure 1, and is similar to that described previously elsewhere[32]. A DC glow discharge plasma was sustained between a flowing solution exiting a quartz capillary (0.38mm I.D. and 1.1mm O.D.), and a pin-type metal counter-electrode (2% lanthanated tungsten). Voltage was applied using a DC power supply (Glassman High Voltage, Series EK) operating in current-control mode, with a 2KΩ 100W ballast resistor set in series between the metal pin electrode and the power supply. A graphite electrode placed in the waste reservoir completed the electrical circuit. Positive polarity potential was applied to the pin electrode in the case of the SCGD experiments, and a negative polarity potential was applied to the metal electrode in the case of the SAGD experiments. A peristaltic pump (Spetec, Perimax 12) was used to provide solution at a flow rate of 2.5mL/min into the quartz

capillary, and the same peristaltic pump was used to remove excess solution from the waste reservoir, maintaining a constant reservoir solution level. Solutions were prepared from high purity 1000 mgL^{-1} standards (Sigma Aldrich) in aqueous 1% HNO_3 solutions made using 18-MOhm ultrapure water (VWR analytical). The voltage drop measured across a 100Ω resistor placed in series with the circuit was used to monitor discharge current, and a high voltage probe (Tektronix, P6015) located between the ballast resistor and the discharge was used to monitor voltage. Applied potentials typically between 800V-1000V supported currents from 40 – 100mA as noted in the text. All experiments occurred in the ambient atmosphere.

A rectangular N42-grade nickel-coated neodymium (NdFeB) permanent magnet (13 mm x 13 mm x 26 mm) with poles located at the ends of the rectangle (North-to-South vector along the long dimension of the rectangle) and with a maximum residual flux density of 1.3T was positioned with its center 3 cm from the plasma, as illustrated in Figure 1. The Biot-Savart law applied to this rectangular magnet estimates a maximum magnetic field strength of 0.1T at the plasma center. The magnet was held in a mount that allowed it to be rotated so that the flux lines oriented either parallel to the electric field, or transverse to the applied electric field. The magnet could also be rotated at a set rate using an external motor (Pine Research, MSR) placed on a translation stage. A rotating encoder was installed on the motor shaft to monitor the rotational rate of the magnet and thereby the magnetic field vector in real time (CUI Devices, AMT112S-V). The encoder trigger was monitored via the oscilloscope and used as a reference for atomic emission and voltage measurements.

Emission from the plasma was collected through a fused silica lens with a 100-mm focal length, and imaged with a 2.6-times magnification onto the entrance slit of a monochromator (Heath Model EU-700, 0.35m Czerny-Turner) equipped with a photomultiplier tube (Model

R1527, Hamamatsu). Photocurrent was amplified using a current-to-voltage converter (Stanford Research, SR570). Emission, voltage, and current measurements were recorded while varying the frequency of the magnet rotation, interelectrode distance, applied current, and the region of the plasma being examined. Photographic images were captured with a digital camera and a 35mm lens (Nikon d5300, Sigma Art f/1.8 lens) and high speed videos captured with a high-speed CCD camera (Kron Technologies, Chronos 1.4). An oscilloscope (Tektronics, TBS1154), a custom computer program (Labview), or a lock-in-amplifier (EG&G 5209) were used to evaluate signal as noted in the text.

Results and Discussion

Figure 2 depicts the influence of the external magnetic field upon the SCGD in a series of photographic images (exposure time = 1/4000s). The discharge structure of the plasma under four different operating conditions with no external magnetic field are shown for comparison in the first column of Figure 2: a typical SCGD, a typical SAGD, a SCGD without use of a capillary, and a SAGD without use of the capillary. The interelectrode distance was maintained at 5mm throughout. The influence of the quartz capillary to act as an anchoring point for the glow discharge is evident, and provides two key benefits. First, this fixed point prevents the plasma and the surrounding sheath from wandering along the liquid surface, improving the precision of emission measurements[21]. Second, the plasma is confined to the capillary surface area (1.1mm O.D., 0.95mm^2), which acts to increase cathodic current density substantially. The formation of filaments contacting the surface of the 1% HNO_3 solution surface are also evident in both SCGD configurations, and are thought to be critical in removing material from the liquid phase into the plasma. Similar filamentation of the cathode glow of the SCGD [1, 2] and anodic pattern formation on open liquid surfaces has been reported previously[2, 43, 44]. As noted by other investigators,

the filamentary structure is a key aspect of the SCGD operation because the modest power of the discharge (approximately 88W) is concentrated in a small cathodic area. Schwartz and coworkers estimated the area of each tendril attachment to the cathode surface to be approximately 50μm in diameter, and therefore at 990V the current density approaches 0.2-0.5A/mm^2 at the liquid surface[1]. Individual spots on the SAGD anode capillary surface suggest a current density much lower than of the SCGD, approximately 0.008A/mm^2 [9], which is similar to that reported by Bruggeman et al. for a similar low current solution-anode discharge (0.005A/mm^2)[2]. Thus, the power density and current density at the liquid surface are much greater than calculated based on simply considering the entire area of this liquid electrode [45].

Figure 2 also shows the same four plasma conditions under the influence of static magnetic field perturbation. In images marked with a quartered circle(⊗), the magnetic field vector is directed out of the page (North to South (N-S) vector oriented out of the page), while the photos marked with a double circle (⊙) were taken with the magnetic field pointed away (North to South (N-S) vector oriented into the page). Figure 2 also includes images taken with the field parallel (or anti-parallel) to the electric field vector, marked with an arrow oriented from North to South. The effect of the Lorentz force on the positive column of the discharge is very evident. The deflection of the positive column in the magnetic field follows the force vector of the Lorentz force on the current of moving electrons. As anticipated, Figure 2 shows that the SCGD deviates in the opposite direction as the SAGD under influence of the same magnetic field. Similarly, the direction of deflection of each plasma type reverses when the magnetic field vector is oriented in the opposite direction. The effect of capillary confinement of the solution-electrode is also evident in Figure 2, as the SAGD and SCGD are shifted a much shorter distance along the liquid surface as compared to the same discharge structures without capillary confinement. When there is no capillary to

confine the solution electrode of the plasma, this region of the discharge moves several mm along the liquid surface. Finally, the plasma appears visually similar when the magnetic field is oriented parallel (or anti-parallel) to the electric field between the electrodes and when the magnetic field is absent.

It is also worth noting that the positive column of the plasma is most affected by the magnetic field (e.g. Figure 2 SCGD), and deflects as much as 5-6mm from the central axis of the plasma upon exposure to the magnetic field. Many reports have confirmed that the SCGD maintains the characteristic spatial distribution of a typical glow discharge[46], and thus given the lower electric field within the positive column and greater region length, it is not surprising that the magnetic force is most evident in that region. Computational simulations reported by Surzhikov and Shang have examined the effects of a transverse magnetic field upon a normal glow discharge structure, and predict the asymmetrical structural of the positive column similar to that observed in Figure 2[47]. The same studies also predicted the shift in location of the discharge from the central axis, and the reverse of the effect when the magnetic field direction is reversed[48]. It is also worth noting that the anchor point of the discharge on the pin electrode (anodic electrode region of the SCGD) also shifts under influence of the magnetic field, and that the discharge anchors to the slopes of the pin electrode in both polarities.

As the magnetic field is rotated with respect to the plasma, each of the orientations depicted in Figure 2 is enacted in series, controlling the motion of the SCGD. Figure 3A is a high-speed speed video taken of the SCGD being modulated with a magnetic field rotation of 600RPM with capillary confinement (Multimedia View), Figure 3B is a high-speed speed video taken of the SAGD being modulated with a magnetic field rotation of 600RPM with capillary confinement (Multimedia View). Figure 3C is a video taken of the SCGD being modulated with a magnetic

field rotation of 600RPM without capillary confinement (Multimedia View), and Figure 3D is a high-speed speed video taken of the SAGD being modulated with a magnetic field rotation of 600RPM with capillary confinement (Multimedia View). Videos in the supplemental materials show both SAGD and SCGD in the absence of magnetic fields for comparison. Figure 3 shows that the plasma responds at a rate proportional to the magnet rotation rate. When the discharge is confined at a capillary (Figure 3A and 3B), the plasma sheath can be seen to fluctuate as a whole while the core of the plasma bends less significantly. When there is no capillary to serve as an anchor point (Figure 3C and 3D), the anode (SAGD) or cathode (SCGD) spots traverse over the solution surface. In this experimental setup, the SCGD anchor locations move in a pendular manner with respect to the central axis. The SAGD anchor points rotate in a similar pendular manner but in the opposite direction, that is, 180^0 out of phase with respect to the SCGD motion. The filaments in the SCGD configuration move much more quickly than the rate of rotation of the magnet and are seemingly random in their paths. Bruggeman has shown that similar individual filaments appear resolved on a timescale less than 100μsec[2], and Schwartz reports that filament are stable at measurement times less than 100nsec, and that these anchor points seem to be responsible for atomic emission[1]. Thus, the cathode spots formed by the SCGD move as a loose group due to the rotating magnetic field but continue to move quickly and apparently randomly relative to one another. In contrast, when the solution is anodic, the plasma filaments appear organized and maintain similar structure while undergoing the magnetic field rotation. Overall, these results show that the magnetic field exerts significant influence on plasma structure and can be used to modulate of the SCGD structure.

In order to examine the effect of the magnetic field on the electrical characteristics of the plasma, time-averaged current-voltage curves were measured under various experimental

conditions. The power supply was operated to maintain constant current in all cases, and current measurements were verified to be within 1% of measured values based upon measurement of voltage drop across a series resistor. Figure 4 compiles current-voltage curves for the SCGD and the SAGD with the magnetic field oriented along different vectors with respect to the electric field of the plasma, using descriptions corresponding to the conditions depicted in Figure 2. For most of the conditions examined, the current-voltage curves were very similar under the applied magnetic field and in the absence of any magnetic field. For example, in Figure 4A the SCGD shows a voltage difference of a maximum of 2% (approximately 20V) for all conditions examined. A slight difference in behavior was observed for both SAGD and SCGD plasma systems with the static magnetic field oriented perpendicular to the electric field (Figure 3C and 3D) when interelectrode distance was 7mm. The observed voltage difference was also found to be significant at lower discharge currents, and may reflect the influence of the Lorentz force upon this lower power discharge.

Rotation of the magnetic field did, however, modify the electrical characteristics of the discharge. In Figure 5, time-resolved voltage traces for the SCGD and SAGD within a magnetic field rotating at 600 RPM are presented at different discharge current levels, and are referenced to the same phase by monitoring the rotating encoder. For clarity, the voltage data is presented offset along the Y axis, and mean voltages are available in the supplemental material. The orientation of the magnetic field is also noted when perpendicular to the electric field of the discharge. The label "N-S" signifies that the North-to-South vector of the magnetic field flux is oriented with the North pole towards the column of the discharge, and the "S-N" label signifies the opposite orientation. The SCGD $V_{pk\text{-}pk}$ modulation was found to be coherent with the frequency of the rotating magnetic field, and increased with applied discharge current from 13V at 50-80mA to 35V at a discharge

current of 110mA. The SAGD voltage modulations were found to be fairly consistent at all currents, which corresponded to a peak-to peak voltage ($V_{pk\text{-}pk}$) of 37V volts. As noted in Figure 5, relatively higher discharge potentials corresponded to perpendicular orientation of the magnetic field vector to the discharge electric field, with the N-S orientation 90-degrees with respect to the electric field yielding greatest overall potential. Figure 5 also shows a slight phase lag from the orientation of the magnet to the electric field. Results included in the supplemental materials (Supplemental Figure 1) show that the voltage modulation increased for both SAGD and SCGD as the interelectrode gap is increased. For example, at an interelectrode distance of 7mm the SAGD experienced a modulation amplitude of $V_{Pk\text{-}Pk}$=100V while the SCGD showed $V_{Pk\text{-}Pk}$=20V, with each discharge at approximately the same power (SCGD-88W, SAGD-80W). Supplemental Figure 2 in the supplemental materials shows that the voltage modulation continues for both SAGD and SCGD across all frequencies investigated (300 RPM to 6000 RPM). Of note, the power supply used here was operated in current-control mode and was monitored during these experiments to ensure that discharge current did not vary by more than 1% throughout these studies. Taken together, these data show that a significant difference exists between the discharge in a static magnetic field and the same discharge within a changing magnetic field. The variation in discharge potential reflects the work required to move the plasma discharge across the discharge gap and the increase in discharge size with deflection under the influence of a magnetic field. Since the emission properties of a plasma are influenced by the electrical characteristics of a plasma, magnetic modulation may provide a pathway to improving atomic emission characteristics.

The influence of the magnetic field on the cathode fall potential was also examined. Figure 6A and 6B plot discharge potential as a function of interelectrode distance (discharge gap) for both the SCGD (80mA) and SAGD (100mA). The overall power of each discharge was similar under

these conditions (SCGD=88W, SAGD=80W). Following the method described by Cservalfi[5], the cathode fall potential was estimated by measuring the discharge voltage as a function of interelectrode distance, and then extrapolating to the y-intercept (zero interelectrode distance). Since the same solution composition and conditions were used throughout, the resistance of the solution was unchanged during the study and provides a valid basis of comparison. The cathode falls were found to be statistically identical at each applied condition; 464±5V for the SCGD and 431±14V for the SAGD. Time-averaged cathode fall potentials for the SCGD and SAGD were found to be unchanged if the magnetic field was oriented N-to-S parallel to the electric field, perpendicular to the electric field, rotated at 600RPM, or removed entirely. These cathode fall potentials are slightly lower than those reported elsewhere[1, 2]. Time-resolved measurement of the discharge voltage is shown in Figures 6C and 6D and show that cathode fall potentials calculated by this method do indeed vary slightly according to the various magnetic field orientation during rotation. Maximal and minimal voltage values occur while the magnetic field is perpendicular to the plasma. These differences are likely due to a change in the effective length of the positive column (i.e. bending) which would change the effective interelectrode distance as compared to a change in the cathode drop potential.

Simulation of charged particle transport in plasmas possessing crossed electric and magnetic fields (ExB) predicts shifts in plasma characteristics based upon the ratio of the cyclotron frequency imposed by the Lorentz force (w) to the gas collision frequency within the discharge (v)[51-54]. In instances where gas collisions dominate ($w/v<<1$), electrons complete only partial cyclotron orbits before collisional dephasing and the transport behavior is considered to be collisionally-dominated. The converse situation ($w/v>>1$) reflects field-controlled transport behavior. The reduced electric field (E/n) and magnetic field (B/n), where n is the neutral number

density, broadly reflect the energy gained by the electrons between collisions, and are convenient indicators of likely changes in plasma characteristics[55]. At a gas temperature of 3000K[19] the average reduced field is calculated to be E/n=60 Td (cf. Table S-2). The local electric field in the cathode drop of the SCGD was measured to be between 4.5 x 10^6 V/m and 5.5 x 10^6 V/m (cf. Table S-1), and the reduced field in the cathode drop is calculated to be E/n=2.5x10^3 Td. The electric field measured in the positive column is much lower (3 x 10^4 V/m), and thus the reduced field is correspondingly lower (E/n =12 Td). Based on the estimated magnetic field strength at the plasma center of 0.1 T, the reduced magnetic field is calculated to be B/n=40 Hx. The results of simulations by Ness et al., White et al., and Dujko et al suggest that these reduced field values place the SCGD within a region where changes in charge particle drift velocity are likely to be collisionally-dominated [49, 50][55]. Under these conditions, drift velocity is decreased and a directional bias is observed in the drift velocity (diffusion coefficient) of the charged particles that is sufficient to shift the plasma spatial distribution. However, the electron energy distribution (mean energy) shows only modest change, and thus no significant changes to spectrochemical plasma characteristics would be expected.

Atomic emission from the SCGD was studied under the effect of a static magnetic field in order to evaluate changes in emission characteristics. As shown in Figure 7A, calibration curves for Ag (Ag I 338nm) and Pb (Pb I 405nm) collected at various magnetic field orientation were only slightly different, with magnet positions transverse to the applied electric field showing slightly decreased sensitivity in most instances, while alignment of the field with the electric field vector provided little change in observed sensitivity. Calculated SCGD limits of detection for Ag ranged from 3.6 µg/L with no magnetic field, to 1.6 µg/L and 1.9 µg/L with the magnetic field vector oriented N-S parallel with the electric field, and 2.9 µg/L and 2.7 µg/L with the magnetic

field oriented N-S perpendicular with the electric field. Figure 7C reports a similar response for Pb I 405nm in the SCGD. Limits of detection for Pb were 137 µg/L without a magnetic field, 117 µg/L and 93 µg/L with parallel fields, and 716 µg/L and 141 µg/L with transverse fields. A slight decrease in background emission was observed when the static field was present in any orientation.

As shown in Figure 7B, the SAGD suffered significant adverse analytical consequences under the static fields. With no magnetic field the LOD for Ag was calculated to be 2.5 µg/L. Under the presence of a static field LODs for Ag were measured to be 7.7 µg/L and 10 µg/L for parallel fields and 8.4 µg/L and 24 µg/L for transverse fields. Figure 7D reports similar findings for Pb. Without a magnetic field, the Pb LOD was 57 µg/L, while with a parallel field the LODs improved to 47 µg/L and 49 µg/L, however they worsened with perpendicular fields to 850 µg/L and 1310 µg/L. Slightly higher background noise is seen with the SAGD with application of the magnetic field, which increases the LODs.

As reported by Zhou, these results confirm that application of a magnetic field can improve LODs in the SCGD, but also show that the reverse is true of the SAGD. However, these outcomes may reflect more on the observation of the plasma as perturbed by magnetic deflection, as compared to significant changes in SCGD excitation characteristics. The optical system collects emission from a region along the center of the SCGD and therefore deflection of the plasma (see Figure 2) out of the observation volume of the optical system may decrease observed emission intensity. It has been shown that while a significant portion of atomic emission from the SCGD is found to originate from the cathode dark space and negative glow regions of this glow discharge, atomic emission is also found to originate from the positive column of the discharge[19, 32]. Thus, the deflection of the plasma structure can have significant effect on quantitative response,

especially in cases where material is removed from the liquid and into the positive column for excitation.

Rotation of the magnetic field was found to significantly influence the time-resolved emission signal from the SCGD. Figure 8A displays several time-resolved emission plots of the Ag I 338nm emission line obtained at 600rpm, each at a different horizontal position in the SCGD and referenced to the same rotational phase. The data shows that observed emission follows the magnetic field rotation, and that the maximum emission modulation occurs approximately 0.75mm from the center of the plasma with a minimum amplitude in the center of the plasma (0 mm). Time-averaged, maximum emission occurs in the center of the plasma. Throughout this discussion, "plasma center" refers to the metal-electrode to capillary central axis.

The emission modulation depth (MD) was calculated as the ratio of the peak-to-peak difference of the ac-component of the emission signal to the waveform average ($MD=V_{pk-pk}/V_{average}$) expressed as a percent. Emission modulation depth for Ag was found to be greater off-center (e.g. 0.75mm MD=130%), as compared to at the plasma axis (e.g. 0.0mm MD=45%). In addition, the phase of the modulated emission shifts 180^0 on either side of the center of the plasma (e.g. 0.75mm vs -0.75mm), as would be expected based on the plasma's pendular motion. Figure 8B reports the influence of discharge current on emission modulation at a distance of 0.75mm from the plasma center. Similar to other reports[5], greater discharge current increased average emission. However, modulation depth was found to decrease with increasing current (e.g. Figure 8B: 50mA = 140% versus 120mA = 88%). Figure 8C depicts the influence of magnetic field rotational frequency, from 600 rpm to 6000rpm, on observed emission. Emission intensity closely follows the magnetic field rotation over all frequencies investigated, although modulation depth decreased slightly at higher frequency (MD=138% at 600rpm versus MD=119% at 6000rpm).

Finally, Figure 8D illustrates the effect of interelectrode distance on modulation amplitude. Modulation of emission was found to increase significantly at larger interelectrode distance (Figure 7D:MD=66% at 3mm, 135% at 5mm, and 163% at 7mm). Identical experiments repeated using iron (Fe I 373.nm) showed the same pattern of modulation and are included in the supplemental material (Supplemental Figure 3). Taken together, these results depict a plasma with a positive column that is physically oscillating across the central axis of the discharge. Modulation depth is greatest when emission is collected near the edge of the quartz capillary, and is maximized when the positive column is of greatest length. Given that the positive column possesses the greatest length, it follows that the greatest deviation from the electric field vector should occur in this region of the glow discharge. As sensitivity does not change markedly with magnetic field modulation (Supplemental Figure 9), the results do not suggest any increase in the rate of transfer of sample from the liquid into the plasma.

The same set of experiments were repeated with the SAGD and the results are shown in Figure 9 in identical format. In Figure 8A, the SAGD shows the same pattern of modulation as the SCGD but to a greater extent. The modulation at the center of the SAGD (MD=22%) was found to be less than observed in the SCGD, however, the depth of modulation -0.75mm from the center of the plasma was greater (MD=167%). Similar to the SCGD, increasing the applied current in the SAGD leads to higher total average emission, but decreases modulation depth (Figure 9B: 60mA MD= 220% versus 120mA MD=136%). As with the SCGD, increasing frequency of rotation decreases the modulation depth (Figure 9D: 600RPM MD=148% versus 6000RPM MD=97%), and larger interelectrode distance increases modulation depth (Figure 8D: 3mm interelectrode distance MD=68%, 5mm interelectrode distance MD=171%, and 7mm interelectrode distance MD=201%).

A series of elements were analyzed in order to determine if emission modulation was element-dependent, and the results are presented as normalized atomic emission signal in Figure 9A for the SCGD and 9B for the SAGD. All elements were investigated under identical conditions: 0.75mm from the center of the plasma with 600RPM magnet rotation frequency, using 5mm interelectrode distance. Applied current was 80mA for the SCGD and 100mA for the SAGD in order to maintain similar power levels in each discharge. The modulation depth was observed to be element dependent, although the pattern of the modulation was similar in all cases and reflected the pendular motion caused by the magnetic field rotation. In the SCGD, modulation depth was element-dependent: MD=179% for Pb I 405nm, MD=101% for Au I 267nm, MD=174% for In I 451nm, MD=97% for Ag I 338nm, MD=326% for Zn I 481nm, MD=90% for Na I 589nm, and 148% for Li I 670nm. The SAGD showed greater modulation depth as compared to the SCGD for every element examined: MD=273% for Pb I 405nm, 478% for In I 451nm, 170% for Ag I 338, 465% for Zn I 481, and 228% for Cd I 361nm. All emission lines investigated modulated in essentially the same phase with respect to one another for both SAGD and SCGD, although to greater or lesser extent. In most instances, modulation depth of atomic emission for an element was greatest in the SAGD, although indium and zinc show slightly greater modulation in the SCGD because of the comparatively low sensitivity for those elements in the SAGD. Several elements were unobservable with the SAGD (e.g., Na, Au, Li), however, this result has previously reported for the SAGD and is thus likely unrelated to the magnetic field[9]. The elements studied were of various mass, excitation energy, oxidation state, boiling point, and melting point. The absence of a clear dependence on any of these variables suggests that modulation of emission seen is due to the physical movement of the bulk plasma.

Experiments examining the effect of the magnetic field on emission from prominent background species were also performed. Two of the main spectral background emission components in the SCGD and SAGD are the vibronic bandheads of N_2 ($C^3\Pi_u \rightarrow B^3\Pi_g$, 337nm) and OH ($A^2\Sigma^+ \rightarrow X^2\Pi$, 306nm). Both were examined and compared to the nearby 338nm (Ag I) emission line, and the results are shown in Figure 11A for the SCGD and Figure 11B for the SAGD. Emission from N_2 and OH were found to modulate with approximately the same pattern as Ag emission in both SAGD and SCGD. Investigation of the modulation of these background emission features were performed as a function of location within the plasma, and are included as Supplemental Figures 4 and 5. Like the atomic emission lines, vibronic emission from N_2 and OH shows little modulation at the center of the plasma but increased modulation farther away from the plasma central axis. A change in phase of 180^0 on either side of the center of the plasma, like atomic emission, was also observed for these species. Interestingly, comparison of normalized atomic emission lines with the background components in Figure 11A and 11B shows that atomic emission and molecular vibronic emission features have a slight shift in the observed phase. In Figure 11A, Ag I 338nm atomic emission is compared with N_2 molecular emission, and shows a clear phase-shift with respect to one another and the magnetic field. In Figure 11A, atomic emission from Ag I 338nm lags that from N_2 by approximately 115-degrees (25 msec at 600RPM), but Ag I 338nm atomic emission falls in phase with OH emission. By contrast, Figure 10B shows that the Ag I 338nm emission shows only a small phase-shift with N_2 emission in the SAGD.

Supplementary Figure 8 compares the time-dependent modulation of atomic emission from Zn I 481nm, In I 451nm, Cd I 361nm, and Pb I 405nm in the SCGD (Supplemental Figure 8A) and SAGD (Supplementary Figure 8B). In Supplementary Figure 8A, In I 451nm, Cd I 361nm, and Pb I 405nm emission modulate in phase with one other and with a phase shift of approximately

78-degrees (17 msec at 600rpm) from molecular nitrogen. Emission from Zn is slightly phase-shifted and delayed with respect to the other elements and N_2 background; 50-degrees with respect to Ag I 338nm, and 151-degress with respect to N_2. In the SAGD response shown in Supplementary Figure 8B, In I 451nm, Cd I 361nm, and Zn I 481nm emission are phase-shifted approximately 40-degrees from N_2 emission (approximately 9msec at 600rpm). However, Pb I 405nm emission shows a response in-phase with N_2, different from the other elements studied. These phase relationships may reflect the location from which atomic emission originates within the plasma. The SCGD is a water vapor based plasma, and thus OH is a most likely tied to removal of liquid water from the sample and subsequent desolvation and excitation in the plasma. In contrast, N_2 is thought to originate from surrounding ambient atmosphere. Indeed, spatially resolved emission studies have reported that N_2 is not abundant in the center of the plasma[56, 57]. The phase-delay of atomic emission from N_2 vibronic emission may reflect the fact that atomic excitation occurs in the same locations and the same time as the removal of the sample from the condensed phase, and thus mirrors the emission pattern of OH. Thus, modulation of observed emission results from the physical deflection of the plasma column by the magnetic field, and the changing region observed by the optical experiment as the plasma moves.

Because the atomic emission lines and spectral background are modulated with the same frequency but observed at different phases in the SCGD, experiments were conducted to determine if lock-in amplification could be used to distinguish emission signal from the spectroscopic background from atmospheric components, and thus improve S/N. A lock in amplifier using the optical encoder as a reference waveform was used to evaluate S/N with the plasma imaged 0.75mm off center and at the magnetic rotation of 600RPM. The limits of detection (LOD) for Ag and Pb were improved slightly using the lock-in amplifier and magnetic modulation; LOD for Ag I 338nm

was 3.6 µg/L under typical conditions and 2.6 µg/L using modulation, and LOD based on Ag I 328nm was 5.7 µg/L under typical conditions and 4.4 µg/L using modulation. Calculated LODs for Pb I 405nm were the same; LOD=58 µg/L under typical conditions versus 54 µg/L using modulation. When using magnetic modulation with the SAGD, LODs increased in all cases studied. The LODs for Ag I 338nm worsened from 2.5 µg/L under typical conditions to 9.7 µg/L using modulation, and for Pb I 405nm from 135 µg/L under typical conditions to 160 µg/L using modulation. These limits of detection for the SCGD are comparable to those previously reported, while SAGD LODs reported here are slightly higher than a prior study, although that study did use an alternate solvent system [58].

The reason for these modest improvements to the LOD are likely two fold. First, emission from off-center plasma location (0.75mm) provides slightly lower sensitivity (Figure 8), which decreases overall S/N. Second, the background emission at each atomic emission line is composed of some contribution from N_2, but also contains a contribution from OH vibronic emission and continuum plasma background (e.g. bremstruhlung and ion-electron recombination) with may vary with more similarly to atomic emission. Indeed, when total blank emission background at the Ag I 338nm atomic emission line was examined (see supplemental Figure 4) it showed a slight modulation in-phase with OH and atomic emission. Thus, continuum contribution to the overall spectral background could not be separated from the atomic emission by phase-resolution. This also explains the slightly larger improvement observed for Ag I 338nm as compared to Pb I 405nm, since the Ag I 338nm emission line lies closer to the N_2 vibronic bandhead. Finally, emission lines and background features were examined to determine if magnetic field modulation caused spectroscopic changes to line width (e.g. Zeeman splitting) that might also explain such results. Supplemental Figure 10 shows spectra recorded for the Ag I 328nm line, the H-Alpha line at

656nm, and the wider spectral region containing N_2 and Ag I 338nm, in static magnetic fields and without a magnetic field. No Zeeman broadening, splitting, or shift in peak shapes were detected within the resolution of this experiment.

Conclusion

The SCGD and SAGD represent a novel approach for atomic emission spectroscopy. The application of a magnetic field to these plasmas was found to profoundly influence the physical structure and analytical characteristics of each plasma. Since the SCGD and SAGD operate under opposite electric-field polarity, the structural changes observed in each plasma were in many ways opposites of one another. Static magnetic fields were found to deflect the positive column of the glow discharge structure according to the Lorentz force, but produced little change in current-voltage characteristics or cathode-drop potentials in either discharge. Rotating magnetic fields created an answering modulation of discharge voltage and atomic emission, although time averaged measurements showed little change as compared to the absence of the magnetic field. Rotation of the magnetic field was shown to create an answering modulation in the atomic emission all elements studied as well as vibronic emission from species responsible for spectroscopic background. Interestingly, molecular emission from molecular nitrogen (N_2) was found to be out of phase with atomic emission in the SCGD, while vibronic emission from OH was seen to modulate in phase with atomic emission. Amplitude of the modulation of atomic emission was also found to be element-specific, although of the same waveform for all elements examined. Use of phase-resolved detection led to a slight improvement in LODs for several elements in the SCGD, but provided poorer LODs in the SAGD.

Magnetic fields and magnetic modulation have proved to be useful in controlling aspects of a variety of plasmas, and magnetic manipulation of plasma-liquid surface interactions may

prove to be a successful approach in both controlling surface location and stabilizing the seemingly chaotic interactions at this interface. These approaches might provide a simple way of increasing the effective surface interaction coverage of similar plasmas along the liquid surface, or to focus plasma treatment at specific locations by magnetic deflection. In the SCGD and SAGD explored here, modulation of the discharge is demonstrated, and evidence seems to indicate that perturbation of the plasma in the magnetic field is predominantly a structural change, as opposed to a change in overall electrical or spectroscopic characteristics, which suggests that plasma species energies are not affected either. More sophisticated magnetic modulation approaches, such as change in orientation, the use of solenoids, or through shaped magnetic fields, may permit targeted exploitation in future work.

Supplementary Material: See supplementary material for measured SCGD cathode fall potentials (Table S1), SCGD atomic emission sensitivities (Table S2), Voltage modulation of SCGD and SAGD discharges (Supplementary Figure S1), Voltage modulation of SCGD and SAGD discharges at different frequencies (Supplementary Figure S2), Effect of magnetic modulation on iron emission (Supplementary Figure S3), Modulation of background emission in the SCGD (Supplementary Figure S4), Modulation of background emission in the SAGD (Supplementary Figure S5), Modulation of atomic emission from various elements in the SCGD and SAGD (Supplementary Figure S6), Comparison of emission from nitrogen in the SAGD and SCGD (Supplementary Figure S7), and effect of magnetic modulation on silver emission at the plasma central axis (Supplementary Figure S8).

Acknowledgements: This material is based upon work supported by the National Science Foundation under Grant No. (CHE-1622531) and by the State University of New York at Buffalo. The authors gratefully acknowledge the contribution of the UB Department of Chemistry Mass

Spectrometry Facility, the UB CAS Machine Shop, and the UB Department of Chemistry Electronic Shop. The authors also thank and acknowledge the ICP Information Newsletter and Professor Ramon Barnes, and Indiana University and Professor Gary Hieftje for the donation and loan of some of the equipment used in this study.

Data Availability: Data available on request from the authors.

References

1. Schwartz, A.J., et al., *Visual observations of an atmospheric-pressure solution-cathode glow discharge.* Talanta, 2012. **102**: p. 26-33.
2. Bruggeman, P., et al., *Dc excited glow discharges in atmospheric pressure air in pin-to-water electrode systems.* Journal of Physics D: Applied Physics, 2008. **41**(21).
3. Pohl, P., et al., *Critical evaluation of recent achievements in low power glow discharge generated at atmospheric pressure between a flowing liquid cathode and a metallic anode for element analysis by optical emission spectrometry.* TrAC Trends in Analytical Chemistry, 2017. **88**: p. 119-133.
4. Bruggeman, P.J., et al., *Plasma–liquid interactions: a review and roadmap.* Plasma Sources Science and Technology, 2016. **25**(5).
5. T. Cserfalvi, P.M., P. Apai, *Emission studies on a glow discharge in atmospheric pressure air using water as a cathode.* Journal of Physics D: Applied Physics, 1993. **26**: p. 2184-2188.
6. Michael R. Webb, F.J.A., Gary M. Hieftje, *Compact Glow Discharge for the Elemental Analysis of Aqueous Samples.* Analytical Chemisty, 2007. **79**: p. 7899-7905.
7. Adamovich, I., *The 2017 Plasma Roadmap: Low temperature plasma science and technology.* Journal of Physics D: Applied Physics, 2017. **50**.
8. Jamróz, P., P. Pohl, and W. Żyrnicki, *An analytical performance of atmospheric pressure glow discharge generated in contact with flowing small size liquid cathode.* Journal of Analytical Atomic Spectrometry, 2012. **27**(6).
9. Greda, K., et al., *Flowing Liquid Anode Atmospheric Pressure Glow Discharge as an Excitation Source for Optical Emission Spectrometry with the Improved Detectability of Ag, Cd, Hg, Pb, Tl, and Zn.* Anal Chem, 2016. **88**(17): p. 8812-20.
10. Yuan, M.P., Xiaoxu; Ge, Fen; Li, Qing; Wang, Ke; Yu, Deng-Guang; Wang, Zheng, *Simplified design for solution anode glow discharge atomic emission spectrometry device for highly sensitive detection of Ag, Bi, Cd, Hg, Pb, Tl, and Zn.* Microchemical Journal, 2020. **155**.
11. Guo, X., et al., *Ultra-sensitive determination of inorganic arsenic valence by solution cathode glow discharge-atomic emission spectrometry coupled with hydride generation.* Journal of Analytical Atomic Spectrometry, 2017. **32**(12): p. 2416-2422.
12. Kondeti, V.S.S.K., et al., *Ag+ reduction and silver nanoparticle synthesis at the plasma–liquid interface by an RF driven atmospheric pressure plasma jet: Mechanisms and the effect of surfactant.* Journal of Vacuum Science & Technology A: Vacuum, Surfaces, and Films, 2017. **35**(6).
13. Schwartz, A.J., et al., *Universal anion detection by replacement-ion chromatography with an atmospheric-pressure solution-cathode glow discharge photometric detector.* Anal Chem, 2013. **85**(1): p. 129-37.
14. Hazel, N., J. Orejas, and S.J. Ray, *Evaluation of solution-cathode glow discharge atomic emission spectrometry for the analysis of nanoparticle containing solutions.* Spectrochimica Acta Part B: Atomic Spectroscopy, 2021. **176**.
15. Wang, Z., et al., *Determination of trace sodium, lithium, magnesium, and potassium impurities in colloidal silica by slurry introduction into an atmospheric-pressure solution-cathode glow discharge and atomic emission spectrometry.* J. Anal. At. Spectrom., 2013. **28**(2): p. 234-240.
16. Schwartz, A.J., et al., *Atmospheric-pressure ionization and fragmentation of peptides by solution-cathode glow discharge.* Chem Sci, 2016. **7**(10): p. 6440-6449.
17. Swiderski, K., et al., *Influence of pH and low-molecular weight organic compounds in solution on selected spectroscopic and analytical parameters of flowing liquid anode atmospheric pressure glow discharge (FLA-APGD) for the optical emission spectrometric (OES) determination of Ag, Cd, and Pb.* Journal of Analytical Atomic Spectrometry, 2018. **33**(3): p. 437-451.

18. Mezei, P., T. Cserfalvi, and L. Csillag, *The spatial distribution of the temperatures and the emitted spectrum in the electrolyte cathode atmospheric glow discharge.* Journal of Physics D: Applied Physics, 2005. **38**(16): p. 2804-2811.
19. Webb, M.R., et al., *Spectroscopic and electrical studies of a solution-cathode glow discharge.* Journal of Analytical Atomic Spectrometry, 2005. **20**(11).
20. Cserfalvi, T. and P. Mezei, *Investigations on the element dependency of sputtering process in the electrolyte cathode atmospheric discharge.* Journal of Analytical Atomic Spectrometry, 2005. **20**(9).
21. Cserfalvi, T.s. and P.l. Mezei, *Subnanogram sensitive multimetal detector with atmospheric electrolyte cathode glow discharge.* Journal of Analytical Atomic Spectrometry, 2003. **18**(6).
22. Levko, D., R.R. Arslanbekov, and V.I. Kolobov, *Multi-scale dynamics of atmospheric-pressure discharges ignited over liquid electrodes.* Journal of Applied Physics, 2020. **127**(4).
23. Moon, D.E. and M.R. Webb, *Imaging studies of emission and laser scattering from a solution-cathode glow discharge.* Journal of Analytical Atomic Spectrometry, 2020. **35**(9): p. 1859-1867.
24. Shirai, N., G. Suga, and K. Sasaki, *Mechanism of droplet generation and optical emission of metal atoms in atmospheric-pressure dc glow discharge employing liquid cathode.* Plasma Sources Science and Technology, 2020. **29**(2).
25. Muller, K.G., *Structures at the electrodes of gas discharges.* Phys Rev A Gen Phys, 1988. **37**(12): p. 4836-4845.
26. XinPei Lu, M.L., *Ignition phase and steady-state structures of a non-thermal air plasma.* J. Phys. D; Appl. Phys, 2003. **36**: p. 661-665.
27. Jamroz, P., K. Greda, and P. Pohl, *Development of direct-current, atmospheric-pressure, glow discharges generated in contact with flowing electrolyte solutions for elemental analysis by optical emission spectrometry.* TrAC Trends in Analytical Chemistry, 2012. **41**: p. 105-121.
28. Pal Mezei, T.C., Mihaly Janossy, *Pressure Dependence of the Atmospheric Electrolyte Cathode Glow Discharge Spectrum.* Journal of Analytical Atomic Spectrometry, 1997. **12**: p. 1203-1208.
29. Huang, R., et al., *Alternating current driven atmospheric-pressure liquid discharge for the determination of elements with optical emission spectrometry.* Journal of Analytical Atomic Spectrometry, 2011. **26**(6).
30. Wang, J., et al., *Time-resolved emission spectroscopy and plasma characteristics of a pulsed electrolyte cathode atmospheric pressure discharge system.* Journal of Analytical Atomic Spectrometry, 2018. **33**(6): p. 1014-1020.
31. Schwartz, A.J., S.J. Ray, and G.M. Hieftje, *Evaluation of interference filters for spectral discrimination in solution-cathode glow discharge optical emission spectrometry.* Journal of Analytical Atomic Spectrometry, 2016. **31**(6): p. 1278-1286.
32. Schwartz, A.J., et al., *Spatially resolved measurements to improve analytical performance of solution-cathode glow discharge optical-emission spectrometry.* Spectrochimica Acta Part B: Atomic Spectroscopy, 2016. **125**: p. 168-176.
33. Zhou, Y.-J., et al., *Sensitivity improvement of solution cathode glow discharge-optical emission spectrometry by external magnetic field for optical determination of elements.* Microchemical Journal, 2020. **158**.
34. K. TRIVEDI, S.T., M. MATTIES, R. SACKS, *Magnetically Tailored Arc and Glow Discharge Plasmas for Atomic Spectroscopy.* APPLIED SPECTROSCOPY, 1987. **41**: p. 833-843.
35. Stoiljković, M.M., et al., *Emission Intensity Enhancement of DC Arc Plasma Induced by External Oscillating Magnetic Field.* Contributions to Plasma Physics, 2007. **47**(10): p. 670-676.
36. Matsuta, H., *Effect of the position of the external magnetic field applied to a glow discharge plasma on the coherent forward scattering spectra in the Faraday configuration.* Spectrochimica Acta Part B: Atomic Spectroscopy, 2019. **160**.

37. Vega, P., et al., *Spectroscopic evaluation of a compact magnetically boosted radiofrequency glow discharge for time-of-flight mass spectrometry.* Anal Bioanal Chem, 2009. **394**(1): p. 373-82.
38. Phillips, C.E.S., *The Action of Magnetised Electrodes upon Electrical Discharge Phenomena in Rarefied Gases* Roy. Soc. Proc., 1901. **64**: p. 172.
39. Hassouba, M.A., *Effect of the magnetic field on the plasma parameters in the cathode fall region of the DC-glow discharge.* THE EUROPEAN PHYSICAL JOURNAL APPLIED PHYSICS, 2001. **14**: p. 131-135.
40. Surzhikov, S.T., *Abnormal Glow Discharge between Two Electrodes on Plane with Transverse Magnetic Field.* Journal of Physics: Conf. Series, 2019. **1250**.
41. Shidoji, E., *Two-Dimensional Self-Consistent Simulation of a DC Magnetron Discharge* Jpn. J. Appl. Phys, 1999. **38**: p. 2131.
42. Hashem, M.S.M., *The effect of a magnetic field on electron mobilityin a D.C. arc plasma.* Journal of quantitative spectroscopy & radiative transfer, 1984. **31**(1): p. 91-95.
43. Verreycken, T., P. Bruggeman, and C. Leys, *Anode pattern formation in atmospheric pressure air glow discharges with water anode.* Journal of Applied Physics, 2009. **105**(8).
44. Trelles, J.P., *Pattern formation and self-organization in plasmas interacting with surfaces.* Journal of Physics D: Applied Physics, 2016. **49**(39).
45. Doroski, T.A., et al., *Solution–cathode glow discharge – optical emission spectrometry of a new design and using a compact spectrograph.* Journal of Analytical Atomic Spectrometry, 2013. **28**(7).
46. Broekaert, J.A.C. and K.G. Reinsberg, *Spectrochemical analysis with DC glow discharges at atmospheric pressure.* Spectrochimica Acta Part B: Atomic Spectroscopy, 2015. **106**: p. 1-7.
47. Surzhikov, S. and J. Shang, *Normal glow discharge in axial magnetic field.* Plasma Sources Science and Technology, 2014. **23**(5).
48. Surzhikov, S.T. and J.S. Shang, *Two-component plasma model for two-dimensional glow discharge in magnetic field.* Journal of Computational Physics, 2004. **199**(2): p. 437-464.
49. Dujko, S., Z.M. Raspopović, and Z.L. Petrović, *Monte Carlo studies of electron transport in crossed electric and magnetic fields in CF4.* Journal of Physics D: Applied Physics, 2005. **38**(16): p. 2952-2966.
50. Dujko, S., et al., *Non-conservative electron transport in CF4in electric and magnetic fields crossed at arbitrary angles.* Journal of Physics D: Applied Physics, 2006. **39**(22): p. 4788-4798.
51. Ness, K.F., *Multi-term solution of the Boltzmann equation for electron swarms in cross electric and magnetic fields* J. Phys. D; Appl. Phys, 1994. **27**: p. 1848.
52. White, R.D., *Benchmark simulations for electron swarms in crossed electric and magnetic fields.* J. Phys. D; Appl. Phys, 1997. **30**: p. 810.
53. Markosyan, A.H., S. Dujko, and U. Ebert, *High-order fluid model for streamer discharges: II. Numerical solution and investigation of planar fronts.* Journal of Physics D: Applied Physics, 2013. **46**(47).
54. Dujko, S., et al., *High-order fluid model for streamer discharges: I. Derivation of model and transport data.* Journal of Physics D: Applied Physics, 2013. **46**(47).
55. Dujko, S., et al., *Benchmark calculations of nonconservative charged-particle swarms in dc electric and magnetic fields crossed at arbitrary angles.* Phys Rev E Stat Nonlin Soft Matter Phys, 2010. **81**(4 Pt 2): p. 046403.
56. Decker, C.G. and M.R. Webb, *Measurement of sample and plasma properties in solution-cathode glow discharge and effects of organic additives on these properties.* Journal of Analytical Atomic Spectrometry, 2016. **31**(1): p. 311-318.
57. Mezei, P. and T. Cserfalvi, *A critical review of published data on the gas temperature and the electron density in the electrolyte cathode atmospheric glow discharges.* Sensors (Basel), 2012. **12**(5): p. 6576-86.

58. Greda, K., et al., *Enhancement of emission from indium in flowing liquid anode atmospheric pressure glow discharge using organic media.* Talanta, 2019. **204**: p. 304-309.

List of Figures

Figure 1: Diagram depicting the SCGD Atomic Emission Spectroscopy Experiment Modified for Magnetic Field Modulation . Arrows shown in the figure describe the rotation of the magnet.

Figure 2: Images showing modulation of the SCGD and SAGD. Image rows from top to bottom: SCGD, SAGD, SCGD without capillary, SAGD without capillary. Image columns from Left to Right: plasma without magnetic field, plasma with magnetic field vectors coming out of the screen(quartered circle), plasma with magnetic field vectors going into the screen(double circle), plasma with magnetic field vectors directed upwards. Associated videos: Multimedia view 2A

Figure 3: High speed videos showing SCGD and SAGD changes due to magnetic field rotation at 600RPM. A) SCGD sustained over a capillary, 80mA, 5mm interelectrode gap (Multimedia Video), B) SAGD sustained over a capillary, 100mA, 5mm interelectrode gap (Multimedia Video), C) SCGD sustained over a capillary, 80mA, 5mm interelectrode gap (Multimedia Video), D) SAGD sustained over a capillary, 100mA, 5mm interelectrode gap (Multimedia Video)

Figure 4: Current-Voltage Curves for SCGD and SAGD in static or rotating magnetic fields. **A**: SCGD; 5mm discharge gap. **B**: SAGD; 5mm discharge gap. **C**: SCGD; 7mm discharge gap. **D**: SAGD; 7mm discharge gap. **E**: SCGD-no capillary; 5mm discharge gap. **F**: SAGD-no capillary; 5mm discharge gap. Orientation of the magnet field in each plot: "North-up" magnetic field vector (N-S) towards pin electrode (parallel to the electric field), "North-toward" magnetic field vector (N-S) towards plasma (perpendicular to the electric field), "600RPM" magnet rotating at 600RPM, "1000RPM" magnet rotating at 1000RPM, and "NoMag" represents absence of any magnetic field.

Figure 5: Discharge voltage influenced by a magnetic field rotating at 600RPM at various discharge currents. **A**: SCGD, **B**: SAGD. Note that voltage traces are offset from one another for clarity of presentation.

Figure 6: Discharge voltage vs interelectrode gap for the SCGD and SAGD. **A**: Time-averaged voltage for SCGD (80mA); **B**: Time-averaged voltage for SAGD (100mA); **C**: Time-resolved voltage for SCGD (80mA); **D**: Time-resolved voltage for SAGD (100mA). "Maxima" and "minima" refer to voltage values at the highest and lowest points of voltage modulation while the discharge was subject to a magnetic field rotating at 600RPM, respectively. "Time averaged" is the average voltage of value of the waveform. Orientation of the magnet field in each plot: "North-up" magnetic field vector (N-S) towards pin electrode (parallel to the electric field), "North-toward" magnetic field vector (N-S) towards plasma (perpendicular to the electric field), "600RPM" magnet rotating at 600RPM, , and "NoMag" represents absence of any magnetic field.

Figure 7: Atomic Emission calibration curves obtained under incluence of magnetic fields. A: SCGD: Ag I 338nm, B: SAGD: Ag I 338nm, C: SCGD: Pb I 405nm, D: SAGD: Pb(I) 405nm. Orientation of the magnet field in each plot: "North-up" magnetic field vector towards pin electrode (parallel to the electric field), "North-Down" magnetic field vector (N-S) towards solution electrode (parallel to the electric field), "North-toward" magnetic field vector (N-S) towards plasma (perpendicular to the electric field), "North-Away" magnetic field vector (N-S) away from plasma (perpendicular to the electric field), "600RPM" magnet rotating at 600RPM, and "NoMag" represents absence of any magnetic field.

Figure 8: Effect of magnetic field modulation on Ag I 338nm emission in the SCGD. **A**: Emission observed at different horizontal locations within the plasma (600RPM, 80mA, 5mm). Plasma center at 0.0 mm refers to the electrode-capillary axis; **B**: Emission observed at different

applied current (600RPM, 5mm, 0.75mm from plasma center); **C**: Emission observed as a function of magnet rotation frequency (5mm, 80mA, 0.75mm from plasma center); **D**: Emission observed at different interelectrode distance (600RPM, 80mA, 0.75mm from plasma center). Note that photocurrent traces are offset from one another for clarity of presentation.

Figure 9: Effect of magnetic field modulation on Ag I 338nm emission in the SAGD. **A**: Emission observed at different horizontal locations within the plasma (600RPM, 80mA, 5mm); **B**: Emission observed at different applied current (600RPM, 5mm, 0.75mm from center); **C**: Emission observed as a function of magnet rotation frequency (5mm, 80mA, 0.75mm from plasma center); **D**: Emission observed at different interelectrode distance (600RPM, 80mA, 0.75mm from plasma center). Note that voltage traces are offset from one another for clarity of presentation.

Figure 10: Modulation of atomic emission from various elements. **A**: SCGD at 80mA, 0.75mm from center, 5mm interelectrode distance, and 600RPM, **B**: SAGD at 100mA, 0.75mm from center, 5mm interelectrode distance, 600RPM

Figure 11: Emission modulation of 10mg/L Ag (black), Nitrogen-337nm (red), and OH-306nm (blue). **A**: SCGD, **B**: SAGD

Journal of Applied Physics

PLEASE CITE THIS ARTICLE AS DOI: 10.1063/5.0046922

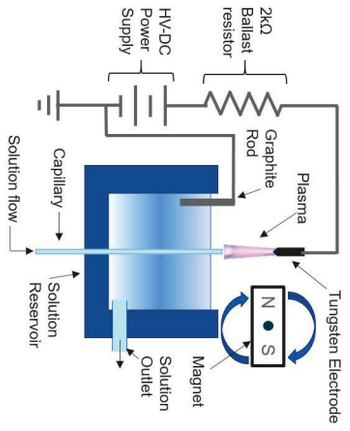

AIP Publishing

Journal of Applied Physics

ACCEPTED MANUSCRIPT

PLEASE CITE THIS ARTICLE AS DOI: 10.1063/5.0046922

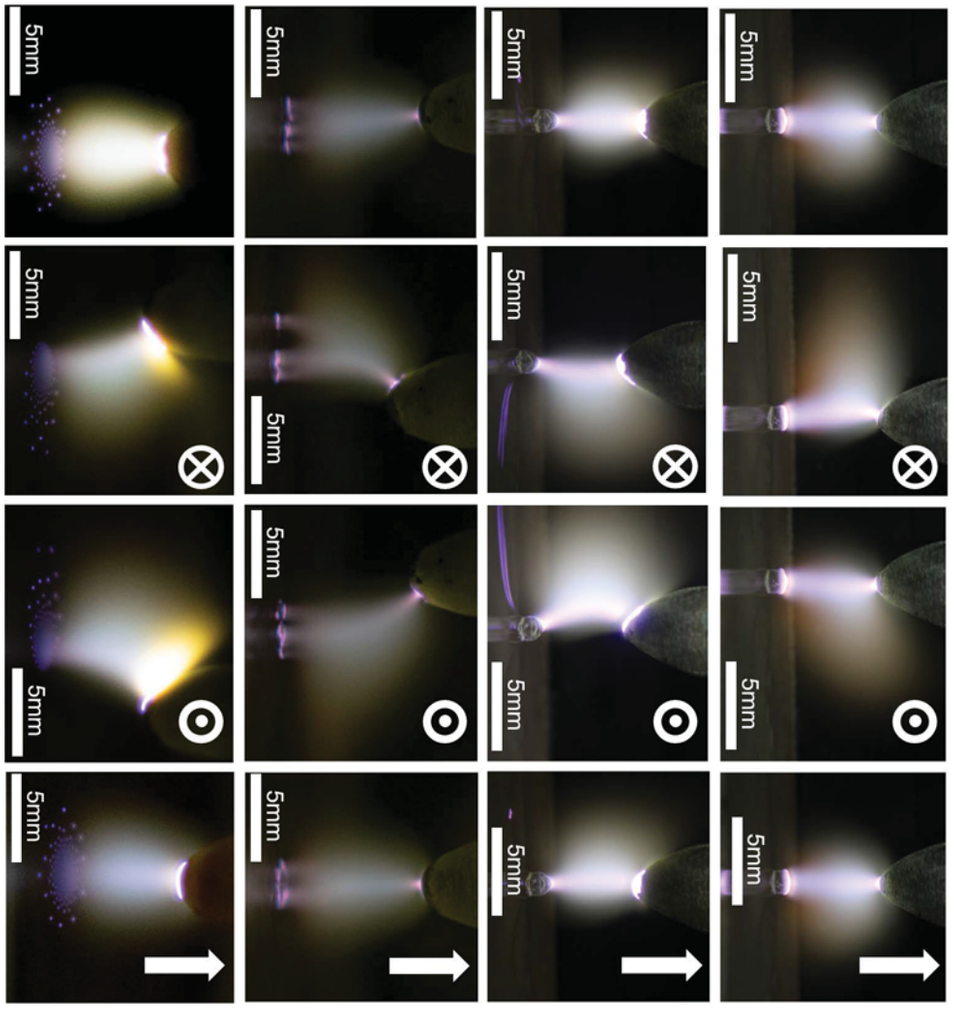

AIP Publishing

Journal of Applied Physics

ACCEPTED MANUSCRIPT

PLEASE CITE THIS ARTICLE AS DOI: 10.1063/5.0046922

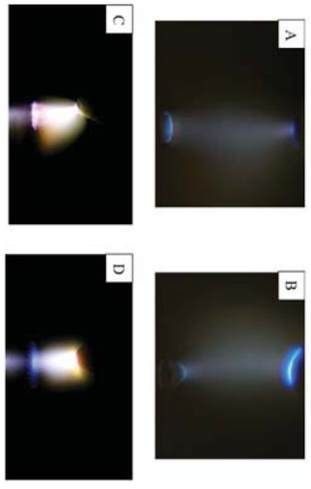

AIP Publishing

Journal of Applied Physics

ACCEPTED MANUSCRIPT

This is the author's peer reviewed, accepted manuscript. However, the online version of record will be different from this version once it has been copyedited and typeset.
PLEASE CITE THIS ARTICLE AS DOI: 10.1063/5.0046922

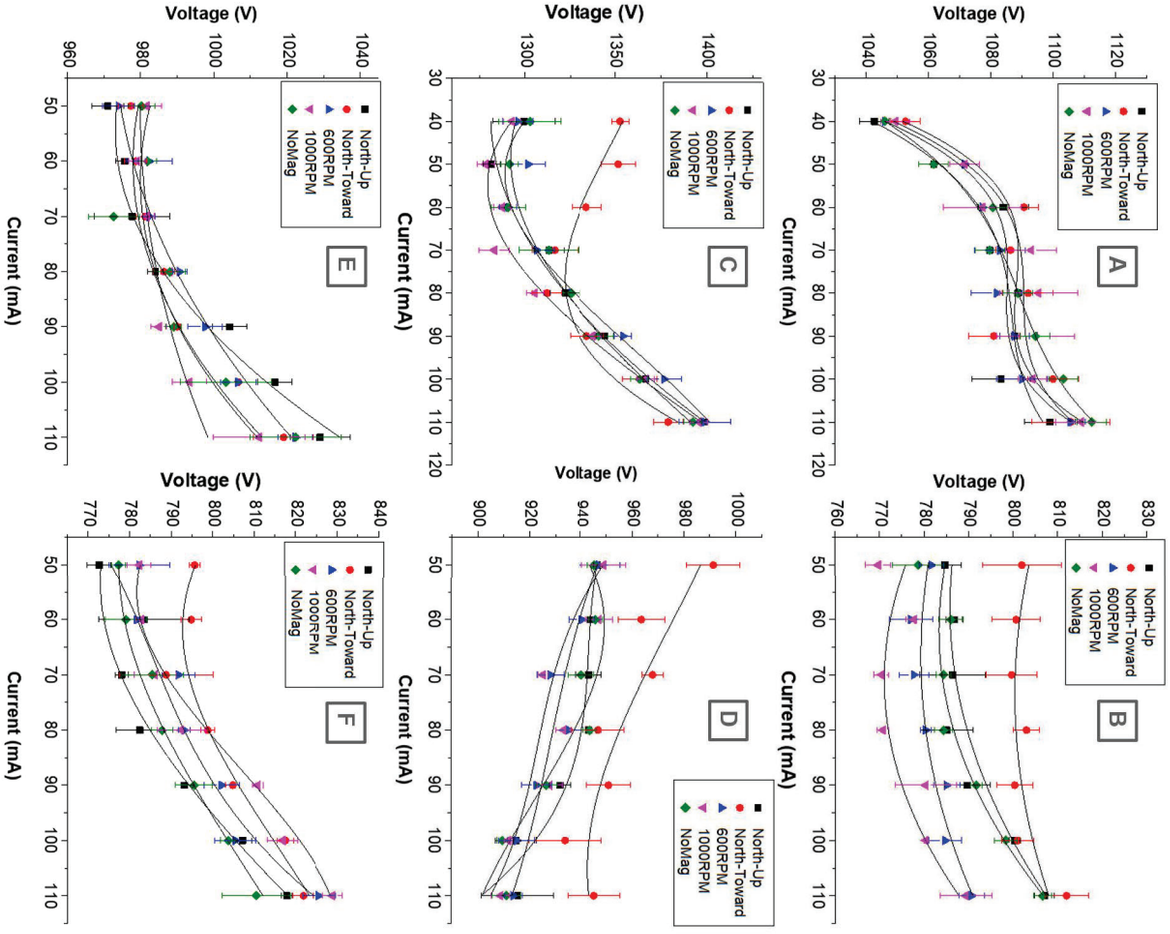

AIP Publishing

Journal of Applied Physics

ACCEPTED MANUSCRIPT

This is the author's peer reviewed, accepted manuscript. However, the online version of record will be different from this version once it has been copyedited and typeset.
PLEASE CITE THIS ARTICLE AS DOI: 10.1063/5.0046922

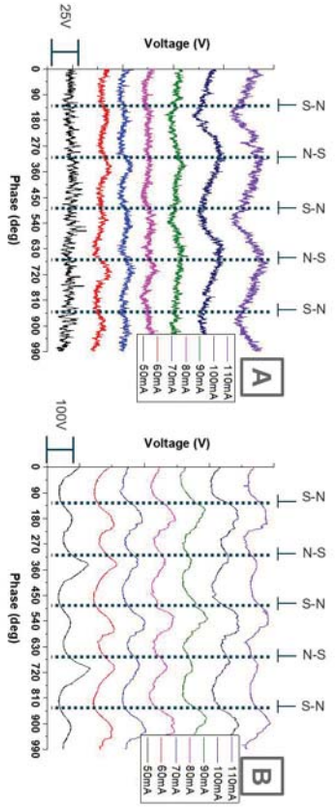

AIP Publishing

Journal of Applied Physics

PLEASE CITE THIS ARTICLE AS DOI: 10.1063/5.0046922

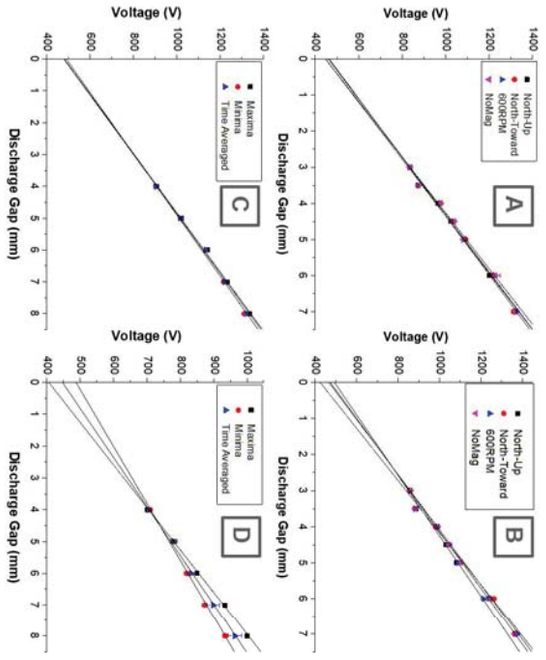

AIP Publishing

Journal of Applied Physics

ACCEPTED MANUSCRIPT

PLEASE CITE THIS ARTICLE AS DOI: 10.1063/5.0046922

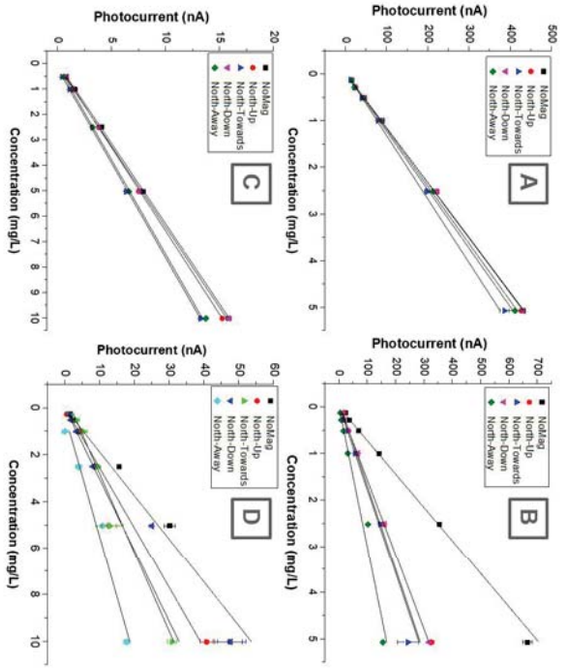

AIP Publishing

Journal of Applied Physics

ACCEPTED MANUSCRIPT

PLEASE CITE THIS ARTICLE AS DOI: 10.1063/5.0046922

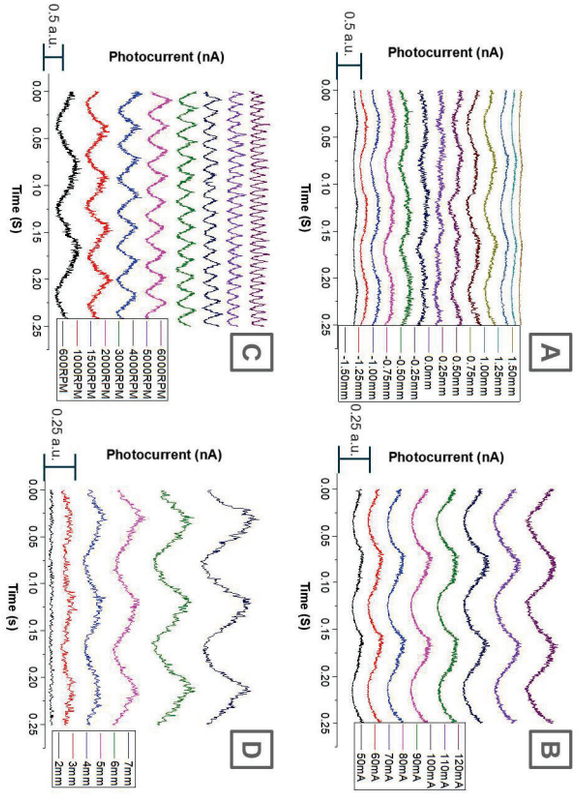

AIP Publishing

Journal of Applied Physics

ACCEPTED MANUSCRIPT

This is the author's peer reviewed, accepted manuscript. However, the online version of record will be different from this version once it has been copyedited and typeset.
PLEASE CITE THIS ARTICLE AS DOI: 10.1063/5.0046922

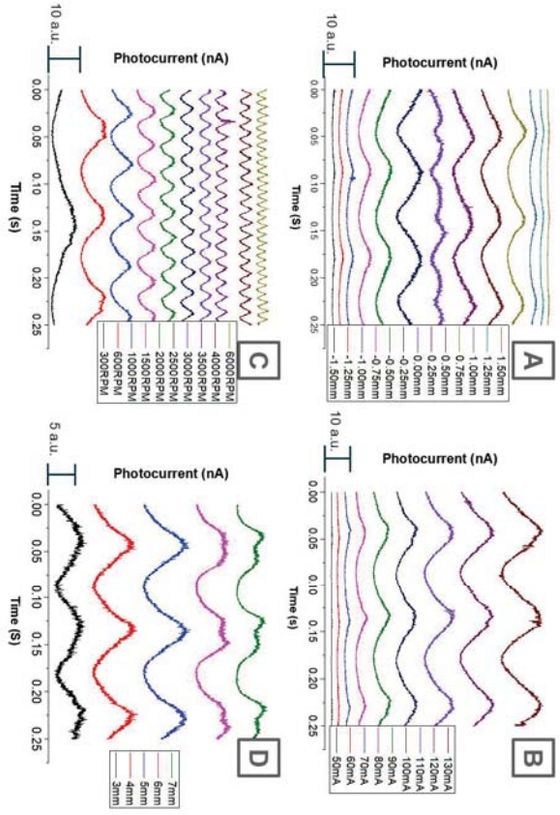

AIP Publishing

Journal of Applied Physics

ACCEPTED MANUSCRIPT

PLEASE CITE THIS ARTICLE AS DOI: 10.1063/5.0046922

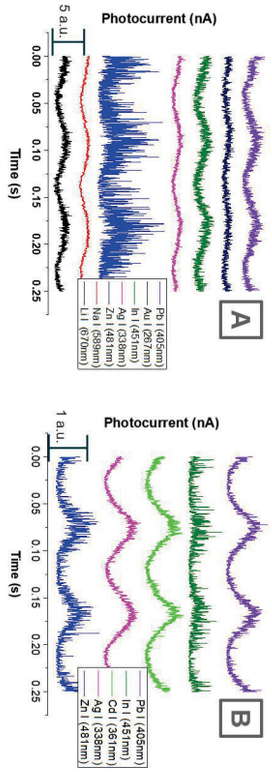

AIP Publishing

Journal of Applied Physics

ACCEPTED MANUSCRIPT

PLEASE CITE THIS ARTICLE AS DOI: 10.1063/5.0046922